Ann Thorac Surg
2011;91:1689–95

Abbreviations and Acronyms

ADC	= apparent diffusion coefficient
DWI	= diffusion-weighted magnetic resonance imaging
^{18}F-FDG	= 18-fluoro-2-deoxy-glucose
FN	= false-negative
FP	= false-positive
GGO	= ground glass opacity
PCNA	= proliferating cell nuclear antigen
PET-CT	= positron emission tomography-computed tomography
ROC	= receiver operating characteristics
ROI	= region of interest
SUVmax	= maximum standardized uptake value
TN	= true-negative
TP	= true-positive

agreed to DWI and PET-CT examinations, were enrolled before operation in this study during the period from May 2009 to October 2010. Patients who had metal or pacemakers in their body or tattoos on the skin were excluded because of contraindication in magnetic resonance imaging (MRI) examinations. Bulky N2 lung cancers with PET or DWI N2 positive lymph nodes were excluded before the enrollment. Patients who received prior treatment for lung cancer were also excluded before the enrollment. This study was approved by the Ethical Committee in Kanazawa Medical University. Written informed consents for MRI, PET-CT, and a pathologic examination of resected materials were obtained from each patient. They underwent DWI and PET-CT examinations before pulmonary resection. Most patients had a preoperative pathologic diagnosis of lung cancer prior to enrollment, and others had a pathologic diagnosis of lung cancer at operation after enrollment. Surgical biopsies of mediastinal lymph nodes through mediastinoscopy were done for assessment of bulky N2 lung cancers and transbronchial needle aspiration biopsy through bronchoscopy were performed to confirm N2 positive lymph nodes. Bulky N2 lung cancers with PET or DWI N2 positive lymph nodes were not candidates for operation but were candidates for induction chemotherapy. Patients who underwent pneumonectomies, bilobectomies, or lobectomies also underwent systematic lymphadenectomies of the hilum and mediastinal areas. Segmentectomy or partial resection for small lung cancers with ground glass opacity was not followed by systematic lymphadenectomies because of the lower possibility of carcinoma metastasis.

Sixty-three patients who had operable lung cancer or who were highly suspected of having lung cancer were enrolled in this study. All of these patients were diagnosed with lung cancer before or during their operation. There were no patients who underwent MRI and PET and then turn out not to have lung cancer. These patients represented 94% of the total number of operation (67) for lung cancers done at our hospital during the period of this study. Forty-one patients were male and 22 patients were female. Their mean age was 68 years old (range, 38 to 81 years). Cell type, cell differentiation, pathologic N factor, and the size of the tumor were determined by reviewing the pathology reports. There were 42 adenocarcinomas, 19 squamous cell carcinomas, 1 large cell neuroendocrine carcinoma and 1 carcinosarcoma. Tumor, nodes, metastasis classification, and the lymph node stations of lung cancer were classified according to the new definition of the International Union Against Cancer 7 [15].

Concerning the clinical T stage (cT), there were 21 cT1a carcinomas, 15 cT1b, 15 cT2a, 3 cT2b, and 9 cT3 carcinomas. In the clinical tumor, nodes, metastasis stage (cStage) by DWI, there were 33 cStageIA, 6 cStageIB, 10 cStageIIA, 4 cStageIIB, 10 cStageIIIA. In the clinical cStage by PET-CT, there were 34 cStageIA, 12 cStageIB, 3 cStageIIA, 4 cStageIIB, and 10 cStageIIIA.

Of the 63 patients enrolled, there were 5 pneumonectomies, 1 bilobectomy, 50 lobectomies, 1 segmentectomy, and 6 partial resections. There were 20 pathologic T1a (pT1a) carcinomas, 14 pT1b carcinomas, 13 pT2a carcinomas, 5 pT2b carcinomas, 8 pT3 carcinomas, and 3 pT4 carcinomas. There were 41 pathologic pN0 (pN0) carcinomas, 11 pN1 carcinomas, and 11 pN2 carcinomas. There were 30 pathologic stage IA (pStage IA), 8 pStage IB, 6 pStageIIA, 3 pStage IIB, 14 pStage IIIA , 1 pStage IIIB, and 1 pStage IV.

MR Imaging

All MR images were obtained with a 1.5 T superconducting magnetic scanner (Magnetom Avanto; Siemens, Erlangen, Germany) with 2 anterior six-channel body phased-array coils and 2 posterior spinal clusters (six-channels each). Patients were in the supine position throughout the examination. Conventional MR images and DWI were acquired during the same procedure. The conventional MR images consisted of a coronal T1-weighted spin-echo sequence (repetition time msec/echo time msec/excitations, 720/20/1) and coronal and axial T2-weighted fast spin-echo sequences (6700/130/1). The T1-weighted and T2-weighted sequences were acquired at a section thickness of 6 mm with a 1-mm intersection gap, and 32-cm field of view with 256 × 192 matrix.

Diffusion-weighted magnetic resonance imaging using a single-shot echo-planar technique was performed under SPAIR (spectral attenuated inversion recovery) with respiratory triggered scan with the following parameters: TR/TE/flip angle, 3,000 to 4,500/65/90; diffusion gradient encoding in 3 orthogonal directions; b value = 0 and 800 s/mm^2; field of view, 350 mm; matrix size, 128 × 128; section thickness, 6 mm; section gap, 0 mm; and number of excitations, 5. Trace images were synthesized for each b value, and ADC maps were automatically produced by the scanner. One radiologist (Y.K.) with 20 years of experience who was unaware of the patients' clinical data evaluated the MRI image. After image reconstruction, a two-dimensional round or elliptical region of interest (ROI) was drawn on the lesion that was detected visually on the ADC map with reference to the T2-weghted image or CT, with exclusion of any necrotic areas. If there

seemed to be no necrotic area, the ROI was placed on the center of the lesion as large as possible. The procedure was repeated 3 times and the mean ADC value was obtained. A receiver operating characteristics curve (ROC curve) was constructed according to the ADC value using GraphPad Prism (version 5.02; GraphPad Software, Inc, La Jolla, CA), and the cutoff values for a diagnosis of metastasis were determined. Lymph nodes with an ADC value of the same or less than the cutoff value were defined as positive by means of DWI. Lymph nodes with an ADC value of more than the cutoff value or those that could not be detected on DWI were defined as negative by means of DWI.

Positron Emission Tomography-Computed Tomography

The PET-CT scanning was performed with a dedicated PET camera (Siemens Biography Sensation 16) before surgery. All patients fasted for 6 hours before scanning. The ^{18}F-FDG (18-fluoro-2-deoxy-glucose) (185 MBq) was administered intravenously. After a 60-minute uptake period, an emission scan was acquired for 3 minutes per bed position and a whole-body scan was performed on each patient using several bed positions according to the height of each patient. One radiologist (M.T.) with 10 years of radioisotope scintigraphy and PET experience who was unaware of the patients' clinical data evaluated the PET-CT data. After image reconstruction, a two-dimensional round ROI was drawn on a slice after visual detection of the highest count on the fused CT image. For the lesions with negative or faintly positive PET findings, the ROI was drawn on the fusion image with the corresponding CT. From those ROI, the maximum standardized uptake value (SUVmax) was calculated as the 18F-FDG accumulation within primary lung cancers and lymph nodes. A ROC curve was constructed according to the SUVmax using GraphPad Prism, and the cutoff values for a diagnosis of metastasis were determined. Lymph nodes with a SUVmax of the same or more than the cutoff value were defined as positive by means of PET-CT. Lymph nodes with a SUVmax less than the cutoff value or those that could not be detected on PET-CT were defined as negative by means of PET-CT.

Statistical Analysis

True-positive, true-negative, false-positive, and false-negative results of DWI and PET-CT for the diagnosis of lymph node metastasis were compared with the results of the pathologic diagnosis. Statistical analysis was performed using StatView for Windows (version 5.0; SAS Institute Inc, Cary, NC). The data are expressed as the mean ± SD. The sensitivity, specificity, and accuracy of DWI versus PET-CT for N staging and diagnosing each lymph node station were compared by using the McNemar test. A p value of less than 0.05 was considered statistically significant.

Results

The ROC curve for the ADC value for diagnosing lymph node metastasis in DWI revealed the optimal cutoff value was 1.70×10^{-3} mm^2/sec (Fig 1A). The ROC curve for the SUVmax for diagnosing lymph node metastasis in PET-CT revealed the optimal cutoff value was 2.40 (Fig 1B). Findings of chest CT, DWI, and FDG-PET of a squamous cell carcinoma are shown in Figure 2.

For detection of primary lung cancers, 61 (97%) of the 63 lung cancers, which consisted of ground glass opacity as well as solid lesions, were detected visually with DWI (Table 1). This was significantly higher than 54 (86%) of the 63 lung cancer detected with PET-CT (p = 0.0207).

The relationships between clinical N factors (cN factors) diagnosed by DWI or PET-CT and pathologic N factors (pN factors) are shown (Table 2). The DWI correctly identified the pathologic N staging in 51 patients (81%), with overstaging in 3 patients (5%) and understaging in 9 patients (14%), giving a staging accuracy of 0.81. On the other hand, PET-CT correctly identified the pathologic N staging in 45 patients (71%), with overstaging in 4 patients (6%) and understaging in 14 patients (22%), giving a staging accuracy of 0.71. The accuracy for N staging by DWI is compared with that by PET-CT

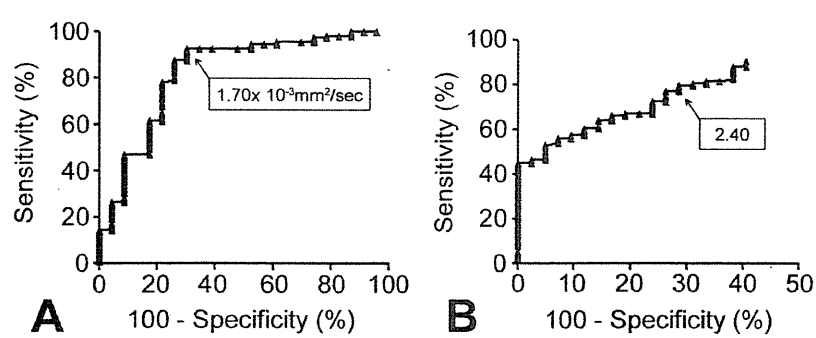

Fig 1. (A) Receiver operating characteristic curve and apparent diffusion coefficient value for diagnosing lymph node metastasis in diffusion-weighted magnetic resonance imaging showing the optimal cutoff value to be 1.70 × 10^{-3} mm^2/second (area under the curve, 0.82; 95% confidence interval, 0.72 to 0.93). Its sensitivity was 0.87 and specificity was 0.74. (B) Receiver operating characteristic curve and standardized uptake value max for diagnosing lymph node metastasis in positron emission tomography-computed tomography showing the optimal cutoff value to be 2.40 (area under the curve, 0.84; 95% confidence interval, 0.77 to 0.91). Its sensitivity was 0.79 and specificity was 0.71.

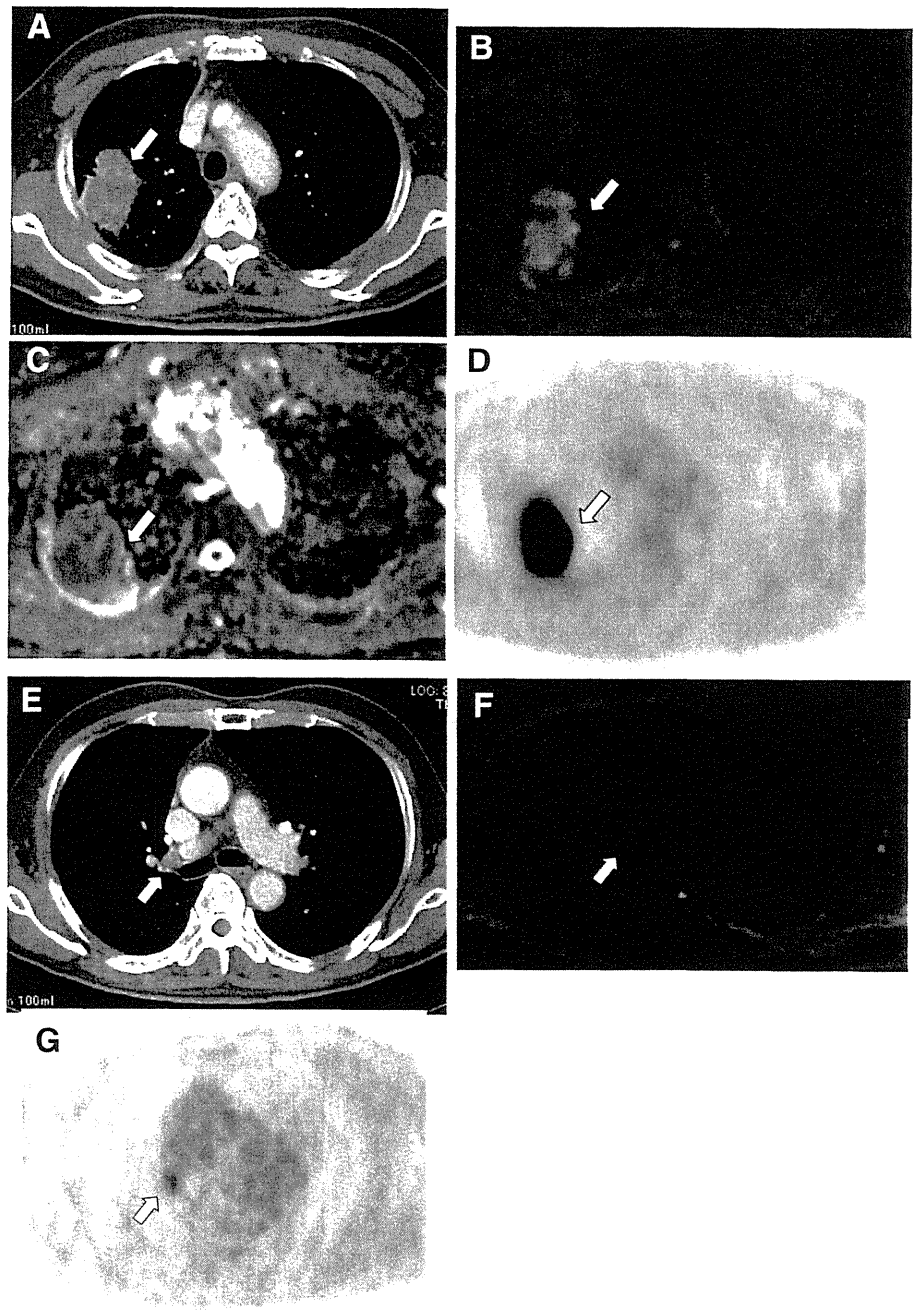

Fig 2. The computed tomography presented lung cancer (arrow) of 55 mm in size in the right upper lobe (A). The DWI showed high signal intensity (arrow) in primary lung cancer (B). The ADC value of the cancer was 0.979 $\times 10^{-3} mm^2$/second (arrow) on the ADC map (C). The FDG-PET showed high accumulation (arrow) in primary lung cancer (D). The SUV max of the cancer was 16.85. The CT showed swelling of #12u lymph node (arrow) (E). The DWI showed high signal intensity in #12u lymph node (F). The ADC value of the node was 1.264 $\times 10^{-3} mm^2$/second (arrow). The FDG-PET showed moderate accumulation (arrow) in #12u lymph node (G). The SUVmax of the node was 3.64. (ADC = apparent diffusion coefficient; DWI = diffusion-weighted magnetic resonance imaging; FDG-PET = fluorodeoxyglucose-positron emission tomography; SUVmax = maximum standardized uptake value.)

using the McNemar test. The accuracy for N staging (0.81 [51 of 63]) by DWI was not significantly higher than that (0.71 [45 of 63]) by PET-CT ($p = 0.0703$). Concerning 11 pN1 carcinomas, the accuracy for N staging (0.64 [7 of 11]) by DWI was not significantly higher than that (0.27 [3 of 11]) by PET-CT ($p = 0.199$). And concerning 11 pN2 carcinomas, the accuracy for N staging (0.55 [6 of 11]) by DWI was not significantly higher than that (0.36 [4 of 11]) by PET-CT ($p = 0.668$).

Of the 319 lymph node stations examined, 44 had metastases and 275 did not. The sensitivity (0.75 [33 of 44]) for metastatic lymph node stations by DWI was significantly higher than that (0.48 [(21 of 44]) by PET-CT ($p = 0.00049$). The specificities of DWI and PET-CT for the 275 nonmetastatic lymph node stations were 0.99 (272 of 275) and 0.97 (266 of 275), respectively. There was no significant difference in the specificities between DWI and PET-CT. The accuracy (0.95 [305 of 319]) for all 319 lymph node stations by DWI was significantly higher than that (0.90 [287 of 319]) by PET-CT ($p = 0.000121$).

The accuracy of the clinical stage was stratified by overall stage. The accuracy (0.71 [45 of 63]) based on DWI

Table 1. Detection of Primary Lung Cancers by DWI and by FDG-PET

Detection	DWI	FDG-PET
Detectable	61 Lung cancers	54 Lung cancers
Not detectable	2 Lung cancers	9 Lung cancers
Detection rate	0.97	0.86

Sixty-one (97%) of the 63 lung cancers were detected visually with DWI. This was significantly higher than 54 (86%) of the 63 lung cancers detected with FDG-PET ($p = 0.0207$).

DWI = diffusion-weighted magnetic resonance imaging; FDG = fluorodeoxyglucose; PET = positron emission tomography.

was not significantly higher than that (0.65 [41 of 63]) based on PET-CT ($p = 0.444$) (Table 3).

There was a weak reverse relationship between ADC value and SUVmax (correlation coefficient, r = 0.286) (Fig 3). There was no relationship between ADC value and tumor size (r = 0.0316).

Concerning the relationship between cell types and ADC value, the ADC value (1.366 ± 0.299) of adenocarcinomas was not significantly higher than that (1.248 ± 0.382) of squamous cell carcinomas. The ADC values were 1.377 ± 0.330 in pN0 carcinomas, 1.278 ± 0.368 in pN1 carcinomas, and 1.187 ± 0.212 in pN2 carcinomas. The ADC values decreased while the pN factor increased but there were no significant differences. Concerning the relationship between cell differentiation and ADC values in adenocarcinomas and squamous cell carcinomas, ADC values increased while the cell differentiation increased. The ADC value (1.037 ± 0.140) of poorly differentiated carcinomas was significantly lower than that (1.275 ± 0.211) of moderately differentiated carcinomas, that (1.336 ± 0.136) of a mixture of moderately and well-differentiated carcinomas, and that (1.415 ± 0.316) of well-differentiated carcinomas. The ADC value (1.125 ± 0.181) of carcinomas with necrosis was significantly lower than that (1.413 ± 0.335) of carcinomas without necrosis. The ADC value (1.314 ± 0.310) of carcinomas without mucus was not significantly lower than that (1.458 ± 0.437) of carcinomas with mucus.

Table 2. Relationships Between Clinical N Factors by DWI or PET-CT and Pathologic N Factors

Clinical N Factor by DWI or PET-CT	Pathologic N Factor		
	pN0	pN1	pN2
DWI			
cN0	38	4	0
cN1	1	7	5
cN2	2	0	6
PET-CT			
cN0	38	7	5
cN1	0	3	2
cN2	3	1	4

DWI = diffusion-weighted magnetic resonance imaging; PET-CT = positron emission tomography-computed tomography.

Table 3. Relationships Between Clinical Stages by DWI or PET-CT and Pathologic Stages

Clinical Stage (cStage) by DWI or PET-CT	Pathologic Stage (pStage)						
	pIA	pIB	pIIA	pIIB	pIIIA	pIIIB	pIV
DWI							
cIA	29	3	1	0	0	0	0
cIB	1	4	1	0	0	0	0
cIIA	0	1	3	0	5	0	1
cIIB	0	0	0	2	2	0	0
cIIIA	0	0	1	1	7	1	0
PET-CT							
cIA	28	3	2	0	1	0	0
cIB	1	5	2	0	3	0	1
cIIA	0	0	1	0	2	0	0
cIIB	0	0	0	1	2	1	0
cIIIA	1	0	1	2	6	0	0

DWI = diffusion-weighted magnetic resonance imaging; PET-CT = positron emission tomography-computed tomography.

Comment

The first aim of this study was to examine the usefulness of DWI compared with PET-CT in the assessment of lung cancer. The current study indicated that DWI is superior to PET-CT in the detection of a primary lesion and nodal assessment of non-small cell lung cancers. There are 3 reasons that indicate the superiority of DWI in comparison with PET-CT. First, the detection rate of carcinoma by DWI was significantly higher than that by PET-CT. It is explained as follows. Solid lesions could be detected both by PET-CT and DWI in this study. Most of the ground glass opacity lesions were not detected by PET-CT but by DWI in this study. It is well known that SUVmax can be lower than the real value when the tumor size is smaller than 20 mm in diameter because of the limited resolution of current PET scanners [16, 17]. The DWI can also be used in place of FDG-PET to distinguish between malignant and benign pulmonary

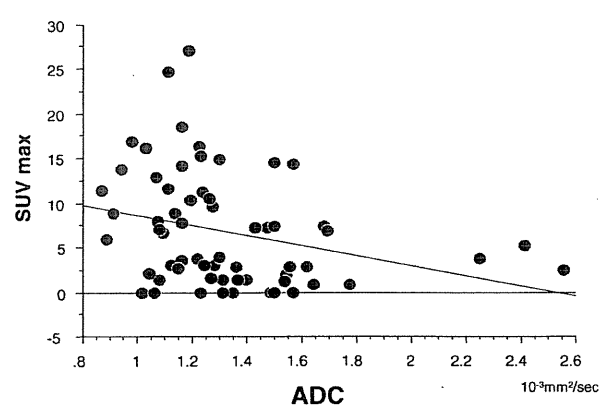

Fig 3. Relationship between apparent diffusion coefficient (ADC) value and maximum standardized uptake value (SUVmax). (SUVmax = 14.297−5.641 × ADC: correlation coefficient, r = 0.286.)

nodules-masses, with fewer false-positive results compared with FDG-PET [14]. These reports support the first reason.

Second, the accuracy of N staging by DWI may be superior compared with PET-CT. In this study the accuracy for N staging (0.81) by DWI was not significantly higher than that (0.71) by PET-CT. Nomori and colleagues [13] reported that the accuracy of N staging in 88 patients was 0.89 with DWI, which was significantly higher than the value of 0.78 obtained with PET-CT because of less overstaging in the former. The superiority of DWI can be explained by the observation that not only did DWI give fewer false-positive results for N staging of non-small cell lung cancer compared with PET-CT [13], but DWI also gave fewer false-negative results for N staging of non-small cell lung cancer compared with PET-CT. The PET-CT is likely to show false-positive results when lymph nodes contain inflammation, and is likely to show false-negative results when the lymph nodes contain a small amount of cancer cells. The DWI with ADC value and signal intensity can be useful in differentiation of malignant and benign mediastinal lymph nodes [18]. Diffusion-weighted magnetic resonance imaging can be used in place of PET-CT for N staging of non-small cell lung cancer, especially in hospitals where MRI examinations can be done but PET-CT examinations cannot. The sensitivity (0.75) of DWI in diagnosing metastatic individual lymph node stations was significantly higher than that (0.48) of PET-CT. The accuracy (0.95) for the lymph node stations by DWI was significantly higher than that (0.90) by PET-CT because of fewer false-negative results in DWI.

Third, the advantages of DWI are easier accessibility, they are relatively cheaper, and there is no X-ray radiation exposure compared with PET-CT. The number of hospitals where PET-CT is equipped is few because of the difficulty in handling the radioisotope of ^{18}F-FDG. The cost of DWI is almost 1/3 of that (about 1,000 US dollars) of a PET-CT examination. In addition, no radiation exposure during a MRI examination is favorable compared with some radiation exposure during a PET-CT examination.

Our results shows that DWI examination is recommended first for staging of lung cancer, and that PET-CT is recommended second for staging of lung cancer. The PET-CT would be recommended first for the assessment of distant metastasis.

The second aim of this study was to examine relationships between the ADC value and several pathologic factors. Although it was reported that there was no significant correlation between ADCmin (the minimum of ADC of total slices within the tumor) and SUVmax or between ADCmean (the average of ADC of total slices within the tumor) and SUVmean (the average of SUV in all voxels) [19], our results showed a weak reverse relationship between ADC of DWI and SUVmax of PET-CT (correlation coefficient, r = 0.286), which was supported by Heo and colleagues [20]. They showed there was a significant correlation between the differentiation and the ADC values of the hepatocellular carcinomas (r = −0.51, p = 0.012).

Although the ADC value of adenocarcinomas was not significantly higher than that of squamous cell carcinomas, the ADC value of adenocarcinoma was reported to be significantly higher than that of squamous cell carcinoma and large cell carcinoma [21]. Well-differentiated adenocarcinomas tended to be hypointense, and small-cell and large-cell neuroendocrine carcinomas showed hyperintensity [22]. The ADC value of lung carcinomas correlated well with tumor cellularity [21]. The DWI signal intensity may be connected with not only the cellularity of tumors, but also the degree of tumor necrosis and mucus, which is speculated from our results.

In this study we evaluated mainly diffusion-weighted MRI and PET in regard to nodal assessment in primary lung cancer. We also recognize another study, which compares diffusion-weighted MRI and PET in regard to malignant and benign lung disease, is necessary. We have started a study dealing with this issue. The history of DWI examination of the lung just began and we need additional data and more information about DWI.

The detection rate of primary lung cancer by DWI may be better compared with that by PET-CT. The accuracy for the lymph node stations by DWI was significantly higher than that by PET-CT because of fewer false-negative results in DWI. The diagnostic efficacy of DWI is superior to that of PET-CT, and DWI can be used in the assessment of lung cancer and lymph nodes instead of PET-CT.

This study was supported partly by a Grant-in-Aid for Scientific Research from the Ministry of Education, Culture, Sports, Science and Technology, Japan (21591828). We are grateful to Mr. Masaru Takahashi and Mr. Keiya Hirata of the MRI Center, Kanazawa Medical University, for technical assistance.

References

1. Dwamena BA, Sonnad SS, Angobaldo JO, Wahl RL. Metastases from non-small cell lung cancer: mediastinal staging in the 1990s–meta-analytic comparison of PET and CT. Radiology 1999;213:530–6.
2. Toloza EM, Harpole L, McCrory DC. Noninvasive staging of non-small cell lung cancer. Chest 2003;123(Suppl 1):137S–46S.
3. Could MK, Kuschner WG, Rydzak CE, et al. Test performance of positron emission tomography and computed tomography for mediastinal staging in patients with non-small-cell lung cancer. Ann Intern Med 2003;139:879–92.
4. Roberts PF, Follette DM, von Haag D, et al. Factors associated with false-positive staging of lung cancer by positron emission tomography. Ann Thorac Surg 2000;70:1154–9.
5. Le Bihan D, Breton E, Lallemand D, Aubin ML, Vignaud J, Laval-Jeantet M. Separation of diffusion and perfusion in intravoxel incoherent motion MR imaging. Radiology 1988; 168:497–505.
6. Tien RD, Felsberg GJ, Friedman H, Brown M, MacFall J. MR imaging of high-grade cerebral gliomas: value of diffusion-weighted echoplanar plus sequences. AJR Am J Roentgenol 1994;162:671–7.
7. Sorensen AG, Buonanno FS, Gonzalez RG, et al. Hyperacute stroke: evaluation with combined multisection diffusion-

weighted and hemodynamically weighted echo-planar MR imaging. Radiology 1996;199:391–401.
8. Schaefer PW, Grant PE, Gonzalez RG. Diffusion-weighted MR imaging of the brain. Radiology 2000;217:331–45.
9. Szafer A, Zhong J, Gore JC. Theoretical model for water diffusion in tissues. Magn Reson Med 1995;33:697–712.
10. Takahara T, Imai Y, Yamashita T, Yasuda S, Nasu S, Van Cauteren M. Diffusion-weighted whole body imaging with background body signal suppression (DWIBS): technical improvement using free breathing, STIR and high resolution 3D display. Radiat Med 2004;22:275–82.
11. Nasu K, Kuroki Y, Kuroki S, Murakami K, Nawano S, Moriyama N. Diffusion-weighted single shot echo planar imaging of colorectal cancer using a sensitivity-encoding technique. Jpn J Clin Oncol 2004;34:620–6.
12. Komori T, Narabayashi I, Matsumura K, et al. 2-fluorine-18 fluoro-2-deoxy-D-glucose positron emission tomography/computed tomography versus whole-body diffusion-weighted MRI for detection of malignant lesions: initial experience. Ann Nucl Med 2007;21:209–15.
13. Nomori H, Mori T, Ikeda K, et al. Diffusion-weighted magnetic resonance imaging can be used in place of positron emission tomography for N staging of non-small cell lung cancer with fewer false-positive results. J Thorac Cardiovasc Surg 2008;135:816–22.
14. Mori T, Nomori H, Ikeda K, et al. Diffusion-weighted magnetic resonance imaging for diagnosing malignant pulmonary nodules/masses: comparison with positron emission tomography. J Thorac Oncol 2008;3:358–64.
15. International Union Against Cancer. TNM classification of malignant tumours. 7th ed. New York, NY: Wiley-Liss; 2009:138–46.
16. Keyes JW Jr. SUV: standard uptake or silly useless value? J Nucl Med 1995;36:1836–9.
17. Mameda M, Higashi T, Kitaichi M, et al. [^{18}F] FDG uptake and PCNA,Glut-1,and hexokinase-II expressions in cancers and inflammatory lesions of the lung. Neoplasia 2005;7:369–79.
18. Kosucu P, Tekinbaş C, Erol M, et al. Mediastinal lymph nodes. Assessment with diffusion-weighted MR imaging. J Magn Reson Imaging 2009;30:292–7.
19. Ho KC, Lin G, Wang JJ, Lai CH, Chang CJ, Yen TC. Correlation of apparent diffusion coefficients measured by 3T diffusion-weighted MRI and SUV from FDG PET/CT in primary cervical cancer. Eur J Nucl Med Mol Imaging 2009;36:200–8.
20. Heo SH, Jeong YY, Shin SS, et al. Apparent diffusion coefficient value of diffusion-weighted imaging for hepatocellular carcinoma: correlation with the histologic differentiation and the expression of vascular endothelial growth factor. Korean J Radiol 2010;11:295–303.
21. Matoba M, Tonami H, Kondou T, et al. Lung carcinoma: diffusion-weighted MR imaging–preliminary evaluation with apparent diffusion coefficient. Radiology 2007;243:570–7.
22. Hayashida Y, Hirai T, Morishita S, et al. Diffusion-weighted imaging of metastatic brain tumors: comparison with histologic type and tumor cellularity. AJNR Am J Neuroradiol 2006;27:1419–25.

Human Pathology (2011) 42, 669–678

ELSEVIER

Human
PATHOLOGY

www.elsevier.com/locate/humpath

Original contribution

Relationship of aquaporin 1, 3, and 5 expression in lung cancer cells to cellular differentiation, invasive growth, and metastasis potential☆

Yuichiro Machida MD[a,b], Yoshimichi Ueda MD, PhD[a,*], Miyako Shimasaki PhD[a], Katsuaki Sato MD, PhD[a], Motoyasu Sagawa MD, PhD[b], Shogo Katsuda MD, PhD[a], Tsutomu Sakuma MD, PhD[b]

[a]*Department of Pathophysiological and Experimental Pathology, School of Medicine, Kanazawa Medical University, Uchinada, Ishikawa 920-0293, Japan*
[b]*Department of Thoracic Surgery, School of Medicine, Kanazawa Medical University, Uchinada, Ishikawa 920-0293, Japan*

Received 17 March 2010; revised 16 July 2010; accepted 23 July 2010

Keywords:
Lung cancer;
Aquaporin 1, 3, and 5;
Invasion and metastasis;
Cellular differentiation

Summary An oncogenic capacity of aquaporins, transmembrane channels for water, was recently proposed. This study seeks to elucidate the involvement of aquaporin 1, 3, and 5 in the development and progression of lung cancer. Expression of aquaporin 1, 3, and 5 was examined by immunohistochemistry, Western blot, and laser-captured microdissection/real-time reverse transcription polymerase chain reaction in 160 lung cancers of various histologic subtypes; and its correlation with clinicopathological factors and survival was analyzed. Aquaporin 1, 3, and 5 were expressed in tumor cells in 71%, 40%, and 56% of lung cancers, respectively. Aquaporin expressions were frequent in adenocarcinomas, whereas aquaporin 1 and 5 were negative in squamous cell carcinomas. Bronchioloalveolar carcinoma cells exhibited an apicolateral aquaporin 1 and apicolateral or basolateral aquaporin 3 localization in nonmucinous type, and apical aquaporin 1 and 5 and basolateral aquaporin 3 expression in mucinous type, which corresponded to aquaporins expression of nonneoplastic lung tissue. Basolateral aquaporin 5 expression was acquired during tumorigenesis of nonmucinous bronchioloalveolar carcinoma. In contrast, invasive adenocarcinoma tumor cells overexpressed aquaporin 1 and 5 with loss of subcellular polarization and with an intracytoplasmic distribution. Overexpression of aquaporin 1 correlated with high postoperative adenocarcinoma metastasis ratios and unfavorable disease-free survival rates (P = .031). We conclude that expression patterns of aquaporin 1, 3, and 5 in lung cancer cells are mostly associated with cellular differentiation. However, the expression of aquaporin 1 and 5 is up-regulated in invading lung cancer cells, particularly in adenocarcinomas; and the overexpression of aquaporin 1 with loss of subcellular polarization is suggested to be involved in their invasive and metastatic potential.

1. Introduction

Aquaporins (AQPs) are a family of small (~30 kd/monomer) channel-forming membrane proteins that function as osmotically driven transepithelial and transcellular water

☆ This study was partly supported by grants HRC 2009-10 (to Y. U.) and S2009-7 (to M. S.) from Kanazawa Medical University, Ishikawa, Japan, and grants 21790369 (to M. S.), 20591678 (to T. S.), and 22590323 (to Y. U.) from the Japanese Ministry of Education, Culture, Sports, Science, and Technology, Tokyo, Japan.

* Corresponding author.
E-mail address: z-ueda@kanazawa-med.ac.jp (Y. Ueda).

0046-8177/$ – see front matter © 2011 Elsevier Inc. All rights reserved.
doi:10.1016/j.humpath.2010.07.022

transporters [1,2]. To date, 13 homologous members have been identified in mammals [3]; and these are expressed by many cell types in different organ systems [4]. Accumulating evidence suggests that AQPs have important roles in various physiological and pathological conditions, such as urinary concentration, exocrine glandular fluid secretion, fat metabolism, and brain edema [5,6]. In peripheral lung tissue, fluid movement between air space and vascular compartments occurs to facilitate absorption of air space fluid as well as in the submucosal bronchial glands for secretion of fluid onto airway surfaces [7]. Water movement in the lung is also vital during development and at birth [8]. At least 4 AQPs, AQP1, 3, 4, and 5, are known to be expressed in the airway and lung [7,9].

Enhanced AQP expression has been reported in tumor cells of different origins, especially aggressive tumors, leading to speculation that AQPs in tumor cells allow water to rapidly penetrate the growing tumor mass [10-14]. Recent studies, however, described previously unanticipated roles for AQPs, including cell cycle control and migration; and evidence supporting the oncogenic roles of AQPs in tumor development, angiogenesis, and cell migration has been obtained [6,15-18]. AQP overexpression has also been shown in lung cancer. However, the significance of this is just beginning to be explored [19-21].

Pulmonary adenocarcinoma (ADC) is the most common and heterogeneous form of primary lung cancer. The recent introduction of high-resolution computed tomography has enabled small peripheral nodular lesions to be detected, providing information on the early stages of peripheral ADC development [22]. However, there remain important issues to be addressed for ADCs, such as what the molecular mechanisms associated with the adverse factors of ADCs are, including invasive growth with fibroblastic reaction, aerogenic spread of a mucinous subtype, and a micropapillary component [22-25]. Little is known about the preferential expression of AQPs in ADC subtypes and their relation to ADC's prognostically adverse factors. In the present study, we examined expression patterns of AQP1, 3, and 5 in lung cancer including various subtypes, as well as nonneoplastic lung tissue, to elucidate the roles of AQPs in the tumorigenesis, cellular differentiation, and invasive growth of ADCs.

2. Materials and methods

2.1. Tissue preparation

A series of 160 surgical specimens from patients with lung cancer were used: 115 were formalin fixed, paraffin embedded for immunostaining of AQP1 and 5; and 45 were frozen OCT compound (Sankyo Co, Tokyo, Japan) – embedded for both immunostaining of AQP3 and quantification of messenger RNA (mRNA) of AQP1, 3, and 5 genes. The samples were selected from the surgical files of Kanazawa Medical University Hospital between 2001 and 2008. Fifteen nonneoplastic lung tissue samples, 10 formalin fixed and 5 frozen, were also obtained for investigation. The Institutional Review Board at Kanazawa Medical University approved this study, and all patients gave their informed consent in writing. The samples included 125 cases of ADCs (98 formalin fixed, 27 frozen samples), 18 squamous cell carcinomas (SCCs) (8 and 10 samples, respectively), 5 large cell carcinomas (1 and 4 samples), and 12 small cell carcinomas (8 and 4 samples). Two samples of atypical adenomatous hyperplasia (AAH) formalin fixed were also included. To determine the role of AQPs in cellular differentiation and invasive growth of ADCs, the samples were subdivided, in addition to original subtypes of 2004 World Health Organization classification [24] and Union for Internation Cancer Control–7 histologic grading of differentiation (G1-4) [26], into the following 5 groups: a pure nonmucinous bronchioloalveolar carcinoma (BAC) group (20 formalin-fixed and 4 frozen samples); a group of a mixed subtype having a predominant BAC component with a focus of invasive ADC, either papillary or acinar (21 and 6 samples, respectively); a group of a mixed subtype of widely invasive well- (G1) to moderately differentiated (G2) ADC, either papillary or acinar, with a small BAC component (26 and 5 samples); a mucinous tumor group, either mucinous BAC or mixed subtype with a predominant mucinous BAC but with small foci of invasive components elsewhere (15 and 4 samples); and a poorly differentiated (G3) ADC group (16 and 8 samples). Micropapillary structures in more than 30% of the tumor tissues were observed in 20 of the 125 ADC cases. The micropapillary pattern was determined according to the criteria of Miyoshi et al [23]; and the continuous linear staining outside of the micropapillary small clusters, suggesting an inside-out growth pattern, was confirmed in all 20 tumors by immunostaining with anti–epithelial membrane antigen (EMA) antibody as described in Section 2.4. Staging was performed according to the revised tumor-node-metastasis staging system for lung cancer [26]. Of 160 cases, 114 were pStage I, 15 were pStage II, 28 were pStage III, and 3 were pStage IV. The median patient age was 65 (31-81) years, there were 67 women and 93 men, and 41.7% had a history of smoking. Follow-up after surgery was from 5 to 92 (mean, 31) months. For each case, the most representative block was selected from a number of paraffin blocks covering at least 1 or 2 maximal cut surfaces.

2.2. Immunostaining for AQP1 and 5

Immunostains for AQP1 and 5 were performed according to Hoque et al [19] and Chae et al [21], respectively, with minor modification. For antigen retrieval, the sections were autoclaved at 121°C for 15 minutes. Tissue sections were incubated overnight at 4°C with affinity-purified anti-AQP1 and AQP5 rabbit polyclonal antibodies (Alpha Diagnostic, San Antonio, TX) at a concentration of 6.7 and 20 μg/mL, respectively. The antibodies applied were visualized using the avidin-biotin-peroxidase technique (DAKO LSAB kit;

Dako Cytomation, Carpinteria, CA) followed by chromogen detection with diaminobenzidine (Dako Cytomation). The sections were counterstained with Meyer hematoxylin. Immunostainings were evaluated by 3 pathologists (Y. U., S. M., and K. S.) blinded to the clinicopathological variables. The expression was defined as positive when greater than 10% of tumor cells showed distinct chromogen reactions.

2.3. Immunostaining for AQP3

The expression and localization of AQP3 were examined on frozen sections using a streptavidin-biotin-peroxidase complex method (Histofine SAB-PO kit; Nichirei, Tokyo, Japan). Frozen tissues were cut into 4-μm–thick sections and fixed in 90% ethanol for 3 minutes. The tissues were incubated for 2 hours at 37°C with rabbit anti-AQP3 polyclonal antibody (Calbiochem, San Diego, CA) at a concentration of 3 μg/mL.

2.4. Immunostaining for EMA, Ki67, TP53, and carcinoembryonic antigen

Immnunostainings for EMA, Ki67, p53, and carcinoembryonic antigen (CEA) were performed on formalin-fixed, paraffin-embedded sections, 20 sections for EMA and 115 sections for Ki67, p53, and CEA, using the avidin-biotin-peroxidase technique (DAKO LSAB kit; Dako Cytomation). Mouse monoclonal antibodies against EMA (Dako Cytomation), Ki67 (clone MIB-1; Takara Bio Inc, Shiga, Japan), p53 (Dako Cytomation), and CEA (IBL Co Ltd, Gunma, Japan) were used as primary antibodies. Pretreatment with autoclave was done for all antibodies. The stainings were evaluated according to Anami et al [27]: Ki67 was judged as positive when nuclear labeling of tumor cells (MIB-1 labeling index) was more than 10%; p53 was judged as positive when nuclear labeling was more than 30%; CEA was judged as positive when cytoplasmic labeling was more than 60%.

2.5. Western blotting

Immunoblotting for AQP1 was performed on 10 representative tumor tissues, 8 cases of ADCs and 2 cases of SCCs, as well as a nonneoplastic lung tissue sample. Proteins were extracted using lysis buffer (50 mmol/L Tris-HCl [pH 7.6], 10% glycerol, 5 mmol/L magnesium acetate, 0.2 mmol/L ethylenediamine tetraacetic acid, 1 mmol/L phenylmethylsulfonyl fluoride, and 1% sodium dodecylsulfate). Extracted protein (10 μg) was applied to and electrophoresed on a 10% polyacrylamide gel and transferred to a nitrocellulose membrane (Atoh, Tokyo, Japan). The membranes were reacted overnight at 4°C with anti-AQP1 polyclonal antibody (Alpha Diagnostic) at a concentration of 2 μg/mL. After the incubation with peroxidase-labeled goat anti-rabbit IgG antibody (Dako Cytomation) for 1 hour at room temperature and vigorous washing, the nitrocellulose membrane was incubated with Chemiluminescence Luminol Reagent (Pierce, Rockford, IL) and photographed digitally using ATTO Light-capture (AE-6971; ATTO, Tokyo, Japan). All samples were standardized by immunoblot using anti–β-actin mouse monoclonal antibody (Sigma Chemical Co, St. Louis, MO).

2.6. Laser-captured microdissection and quantitative gene expression analysis using real-time reverse transcriptase polymerase chain reaction

Laser-captured microdissection (LCMD) was used to collect tumor cells from 16 fresh-frozen lung carcinoma tissues as well as nonneoplastic lung cells using a previously described procedure [28]. Tumor cells were dissected and collected using a PALM laser microdissection system (Meiwa Shoji Co, Tokyo, Japan). In nonneoplastic lung tissues, bronchial epithelia and alveoli composed of both alveolar cells and capillaries were dissected. Real-time reverse transcriptase polymerase chain reaction (RT-PCR) was performed using a TaqMan One-Step RT-PCR Master Mix Reagents Kit (PE Applied Biosystems, Branchburg, NJ). TaqMan probes for AQP1, 3, and 5 were purchased from Assays-on-Demand Gene Expression Products (Applied Biosystems, Foster City, CA). The accession numbers and sequences of the probes were as follows: Hs01028916, FAM-CGG TCC TTT GGC TCC GCG G for AQP1; Hs01105468, FAM-TGG GCT CCA TTG CGG GTG TCT TC for AQP3; and Hs00893081, FAM-GCT ACC CCA GAA AAC CCA GTG AGC for AQP5. Glyceraldehyde-3-phosphate dehydrogenase (GAPDH) gene expression was used as an internal control for standardization. The TaqMan probe for GAPDH gene was Hs99999905, FAM-GGGCGCCTGGTCACCAGGGCTGCTT (Assays-on-Demand Gene Expression Products, Applied Biosystems). The relative amount of the specific amplification product of the sample was calculated using a standard curve created with complementary DNA solution produced from BD qPCR Human Reference Total RNA (Applied Biosystems), and standardized according to the amount of GAPDH. All processes were performed in triplicate.

2.7. Statistical analysis

The clinical end points examined were the time from treatment initiation to the time of metastasis (disease-free survival). For comparisons between AQP expression and clinicopathological factors, the χ^2 test was used. Prognostic factors were examined by both univariate and multivariate analyses. The disease-free survival rates were calculated using the Kaplan-Meier method and compared with the log-rank test. A P value of $< .05$ was considered statistically significant. All statistical analyses were performed using StatView software (SAS Institute Inc, Cary, NC).

3. Results

3.1. Expression of AQP1, 3, and 5 in nonneoplastic lung tissue

In nonneoplastic lung tissues, AQP1 was constantly expressed in the vasculature and apicolateral surfaces of type II pneumocytes, particularly those that were proliferating (Fig. 1A), and apical surfaces of bronchial/bronchiolar surface epithelium (BSE), whereas surfaces of goblet cells were negative for AQP1. Plasma membranes of myoepithelial cells surrounding bronchial glands and red blood cells also showed AQP1 expression. AQP3 expression was detected in basolateral plasma membranes of BSE and in whole plasma membranes of basal cells of the bronchus, as well as the apicolateral surfaces of type II pneumocytes. The apical surfaces of BSE except for goblet cell areas (Fig. 1B), apicolateral membrane of bronchial gland cells, and type I pneumocytes (Fig. 1C) were positive for AQP5 expression. Areas of bronchial squamous metaplasia and reactive type II pneumocytes showed negative for AQP5.

3.2. Expression of AQP1, 3, and 5 in lung cancer

AQP1, 3, and 5 expression was detected in tumor cells of 71%, 40% and 56% of lung cancers, respectively. Positive expression ratios were high in well- (G1) to moderately differentiated (G2) ADCs (83%, 64%, and 70%, respectively), but lower in poorly differentiated (G3) ADCs (56%, 13%, and 44%, respectively) and undifferentiated carcinomas (G4) (44%, 25%, and 11%, respectively). AQP1 and 5 expression was negative in SCC cells ($P < .001$ in AQP1 and 5), whereas AQP3 was positive in 3 (30%) of 10 cases. Of ADCs, BAC of nonmucinous type, as well as AAH, exhibited distinctive apicolateral AQP1 localization, a basolateral AQP5 expression, and either an apicolateral or basolateral AQP3 expression (Fig. 2A, G-I). BAC of mucinous type showed discontinuous apical expression of AQP1 and 5 except for the surface of goblet cell-type tumor cells (Fig. 2B) and a basolateral expression of AQP3. Invasive ADC tumor cells, having either an acinar component with fibroblastic reaction or papillary and micropapillary components proliferating intraalveolarly, and occasionally those of poorly differentiated carcinomas, exhibited stronger expression of AQP1 and 5 around individual tumor cells without localization in either apicolateral or basolateral plasma membranes (Fig. 2C-F, J), compared with those of nonneoplastic lung tissue and BAC. Invasive tumor cells also showed intracytoplasmic AQP expression in addition to the membranal pattern (Fig. 2C-F, J). A BAC component showing lepidic growth along the preexisting alveolar structure of a mixed subtype showed either a polarized or overexpression pattern for AQP1 and 5. In poorly differentiated ADCs, invading tumor cells associated with a fibroblastic reaction strongly

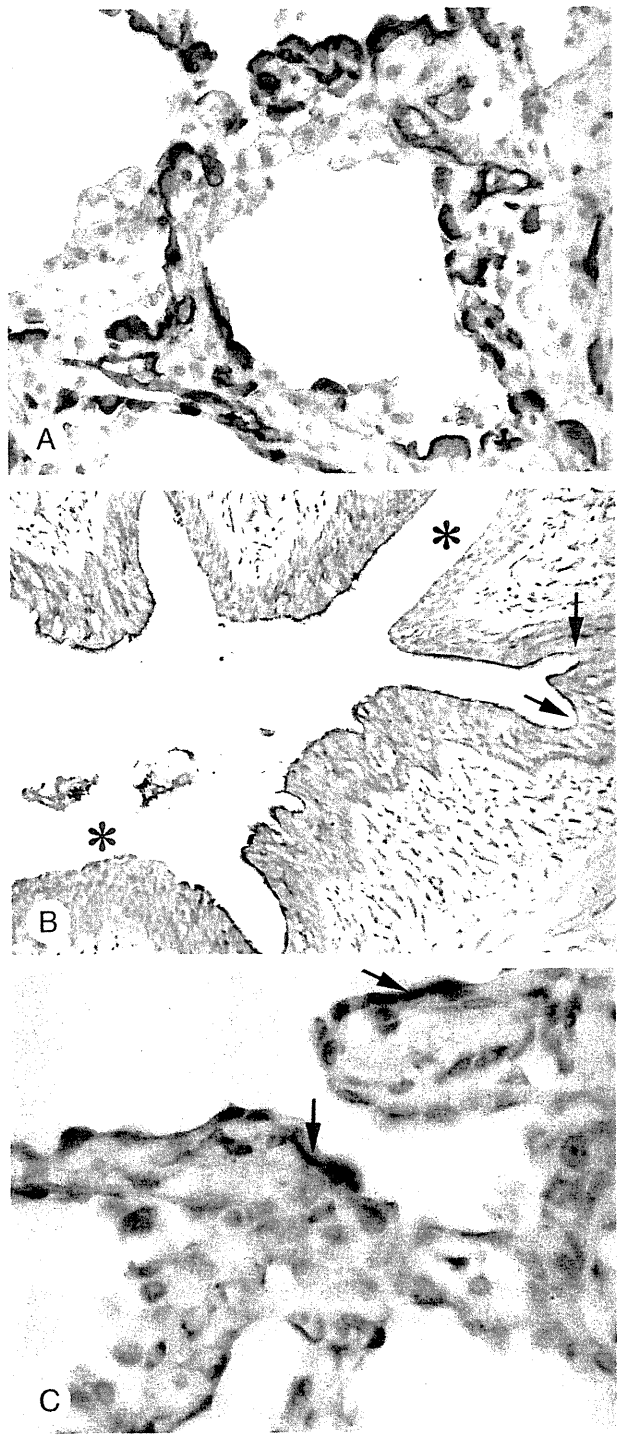

Fig. 1 A to C, Expression of AQP1 and 5 in nonneoplastic lung tissue. A, AQP1. B and C, AQP5. Original magnification: A, ×400; B, ×200; C, ×600. AQP1 is positive in apicolateral surfaces of type II pneumocytes as well as vasculature (A). AQP5 is localized to apical surfaces of bronchial surface epithelium (B) except for areas of goblet cells. Arrows and asterisks (*) show goblet cells and squamous metaplasia, respectively. C, AQP5 expression in type I pneumocytes as arrows indicate, but negative reaction in reactive type II pneumocytes covering the alveolar surface.

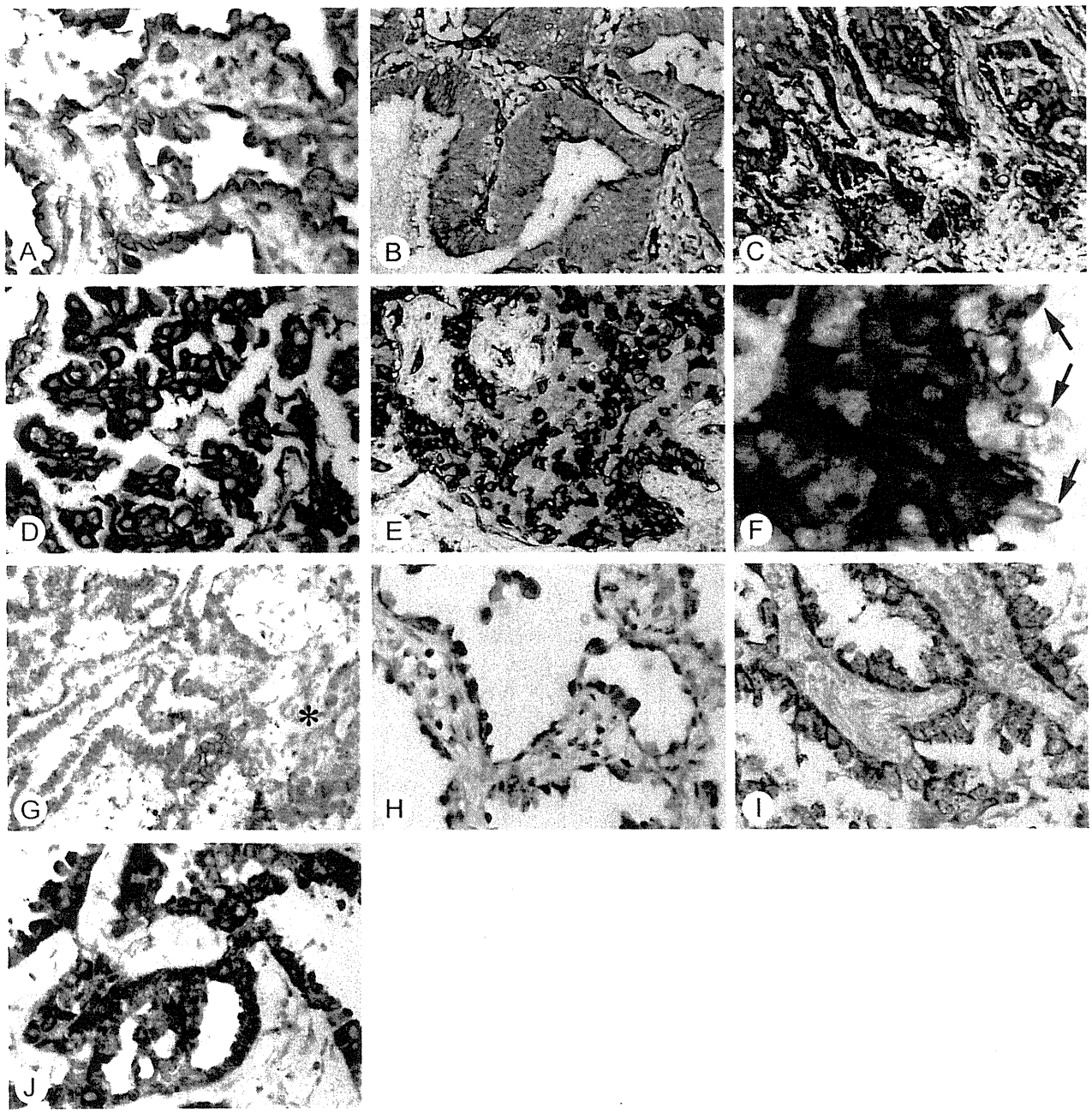

Fig. 2 A to J, Expression of AQP1, 3, and 5 in lung cancer. A to F, AQP1. G, AQP3. H to J, AQP5. A and I, BAC of nonmucinous type. B, BAC of mucinous type. G, ADC of predominant BAC with a focal invasive ADC component. C, D, and J, Widely invasive well- to moderately differentiated ADC. D, A micropapillary ADC component. E, Invasive poorly differentiated ADC. F, Lamellipodia at the invasion front. H, AAH. Original magnifications: A, B, D, H, I, and J, ×400; C, E, and G, ×200; F, ×1000. Nonmucinous BAC cells show apicolateral AQP1 and basolateral AQP3 and 5 expression (A, G, I), and mucinous BAC cells show discontinuous apical AQP1 expression except for the surface of goblet cell-type tumor cells (B). AAH also shows basolateral expression of AQP5 (H). Invasive ADC cells, including micropapillary components (D), show overexpression of AQP1 and 5 with loss of polarization and with intracytoplasmic expression (C-F, J), whereas AQP3 expression decreases (* in G). Arrows in F indicate lamellipodia in the invading edge.

expressed AQP1 (Fig. 2E), whereas in expansively growing tumor cells replacing alveolar space, AQP1 was almost entirely absent ($P < .01$). Lamellipodia structures were seen at the leading edge of invasive tumor cells with fibroblastic reaction, which exhibited a positive reaction for AQP1 (Fig. 2F). In contrast, the immune reaction to AQP3 was weaker or negative in invasive ADC cells (Fig. 2G) compared with that of the BAC component, although loss of the subcellular polarization pattern was detected in half of the positive cases. In undifferentiated carcinoma, small

cell carcinoma expressed AQP1 in 3 of 8 cases, AQP3 in 0 of 4 cases, and AQP5 in 1 of 8 cases, whereas large cell carcinoma showed AQP 1 in 1 of 1 case, AQP 3 in 2 of 4 cases, and AQP5 in 0 of 1 case. Ratios of expression patterns of AQP1, 3, and 5 in histologic subtypes and ADC subgroups were summarized in Fig. 3A-C.

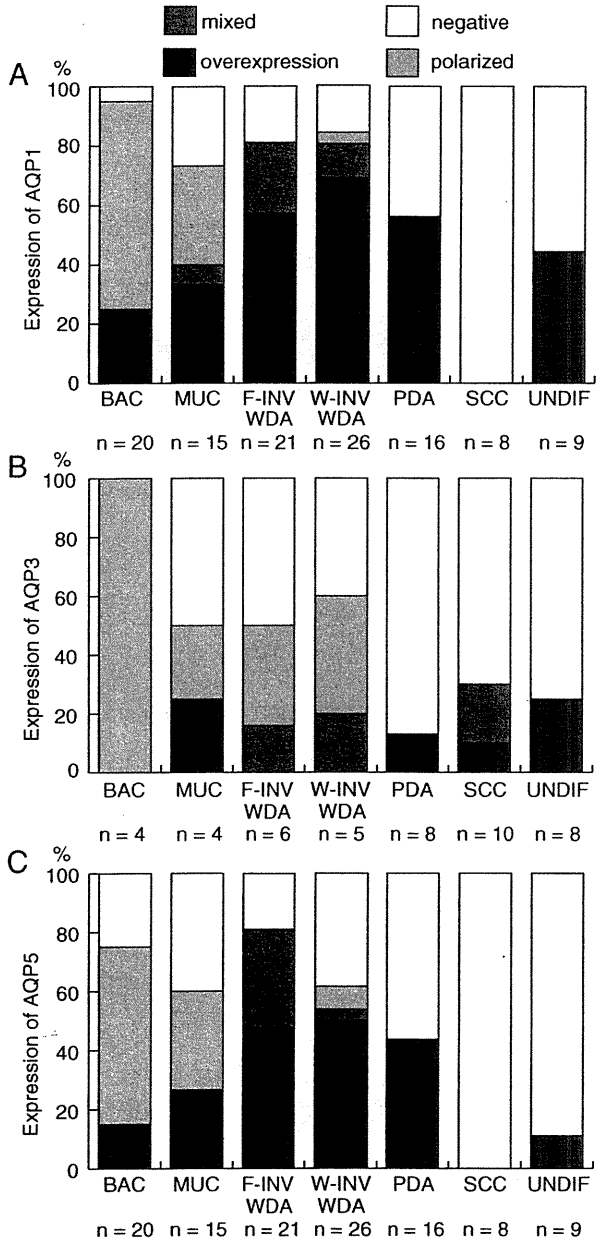

Fig. 3 A to C, Frequencies of the expression patterns of AQP1, 3, and 5 in tumor cells of different lung cancer subtypes. Abbreviations: MUC, mucinous tumor, either BAC or mixed subtype; F-INV WDA, focally invasive ADC of mixed subtype with a predominant BAC component; W-INV WDA, ADC of mixed subtype comprising widely invasive well to moderately differentiated ADC component; PDA, poorly differentiated ADC; UNDIF, small and large cell carcinoma.

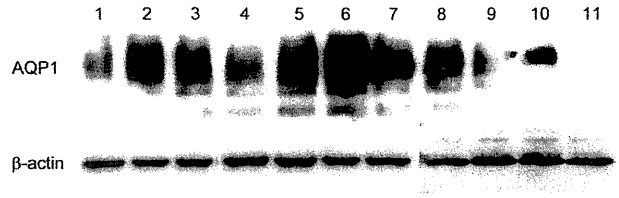

Fig. 4 Western blot for AQP1 in lung cancer of different subtypes and nonneoplastic lung tissue. Lane 1, nonneoplastic lung; lanes 2 and 3, BAC; lanes 4 and 5, ADC of mixed subtype with a predominant BAC component; lanes 6 and 7, ADC of mixed subtype with widely invasive component; lanes 8 and 9, poorly differentiated ADC; lanes 10 and 11, SCC. Expression of AQP1 is shown with a molecular weight of about 30 kd. Increased expression is demonstrated in ADC tissues, particularly in widely invasive cancers, compared with those of nonneoplastic lung tissue and SCCs.

3.3. Western blot for AQP1

An approximate molecular weight of around 30 kd for AQP1 was demonstrated by Western blot analysis. AQP1 was overexpressed in lung cancer tissues, except for SCC, compared with that in nonneoplastic lung tissue. AQP1 expression was particularly increased in invasive ADCs (Fig. 4).

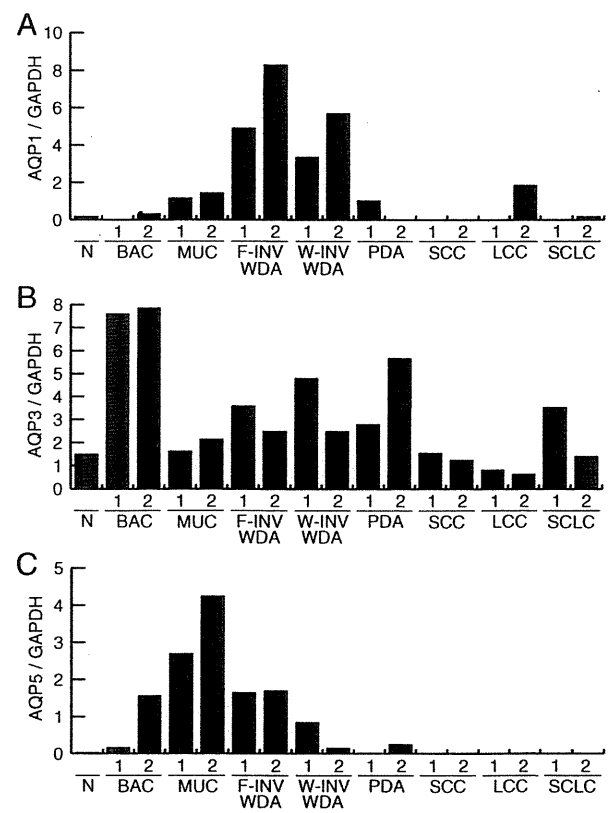

Fig. 5 A to C, AQP1, 3, and 5 mRNA expression in tumor cells of lung cancer of different subtypes and nonneoplastic lung tissue. Abbreviations: N, nonneoplastic lung tissue; LCC, large cell carcinoma, SCLC, small cell lung carcinoma.

3.4. AQP1, 3, and 5 mRNA levels

mRNA of AQP1, 3, and 5 gene expression by the corresponding tumor cells was detected quantitatively by LCMD/real-time RT-PCR. AQP1 and 5 mRNA levels were increased in invasive ADC and mucinous carcinoma cells (Fig. 5A, C). In contrast, the AQP3 mRNA level was high in BAC cells and decreased in invasive ADC and mucinous carcinoma cells (Fig. 5B).

3.5. Prognostic implication of AQP overexpression

AQP1 overexpression with loss of polarization was positively correlated with increased postoperative metastasis ratios in lung cancers (P = .017), particularly in ADC (P = .004) (Table 1). AQP1 showed a significant relationship with postoperative metastatic ratios in stage I cases (P = .024), but it was marginal in stage II to IV cases (P = .061). Tumors overexpressing AQP1 resulted in significantly higher ratios of postoperative metastasis in mucinous ADCs and ADCs with a micropapillary ADC component (P = .011 and .014, respectively) (Table 1). By Kaplan-Meier analysis, patients with AQP1 overexpression with loss of polarization showed a significantly less favorable disease-free survival rate compared with those without it (Fig. 6A, log-rank test P = .031). The adverse effect of AQP1 overexpression on disease-free survival rates was particularly evident in ADC cases with a micropapillary ADC component, although a log-rank score could not be obtained because no metastasis events occurred in patients without AQP1 overexpression (Fig. 6B). AQP1 overexpression was proven to be a significant prognostic factor (P = .041), as well as stage, histologic differentiation, and MIB-1 labeling index (P < .001, P = .041, and P = .038, respectively), of lung cancer by univariate analysis (Table 2). In Cox multivariate analysis including all cases (n = 115), only stage was an independent prognostic factor (P < .0001); and AQP1 overexpression was not (P = .148). However, further analysis in a subgroup consisting of stage I and II cases (n = 95) stratified by age, sex, smoking history, tumor size, and histologic differentiation showed a marginal independent prognostic significance

Table 1 Summary of the correlation of overexpression of AQP1, 3, and 5 with postoperative metastasis ratios in histologic subtypes and ADC subgroups

	Overexpression of AQP	Postoperative metastasis (+)	Postoperative metastasis (−)	P value
AQP1				
All cases	+	17	44	.017*
	−	5	49	
ADC	+	15	33	.004†
	−	4	47	
BAC	+	0	5	.999
	−	0	15	
F-INV WDA	+	1	14	.999
	−	0	6	
W-INV WDA	+	6	8	.081
	−	1	11	
PDA (G3)	+	3	4	.631
	−	3	6	
MUC	+	4	2	.011*
	−	0	9	
ADC with MPA component	+	4	4	.014*
	−	0	12	
SCC	+	0	0	.999
	−	0	8	
Undifferentiated carcinoma (G4)	+	2	2	.523
	−	1	4	
AQP3				
All cases	+	8	10	.462
	−	15	12	
AQP5				
All cases	+	8	50	.335
	−	12	45	

Abbreviations: F-INV WDA, ADC of mixed subtype with a predominant BAC component; W-INV WDA, ADC of mixed subtype with a widely invasive component; MUC, mucinous tumor; PDA, poorly differentiated ADC; MPA, micropapillary ADC.

* P < .05.

† P < .01.

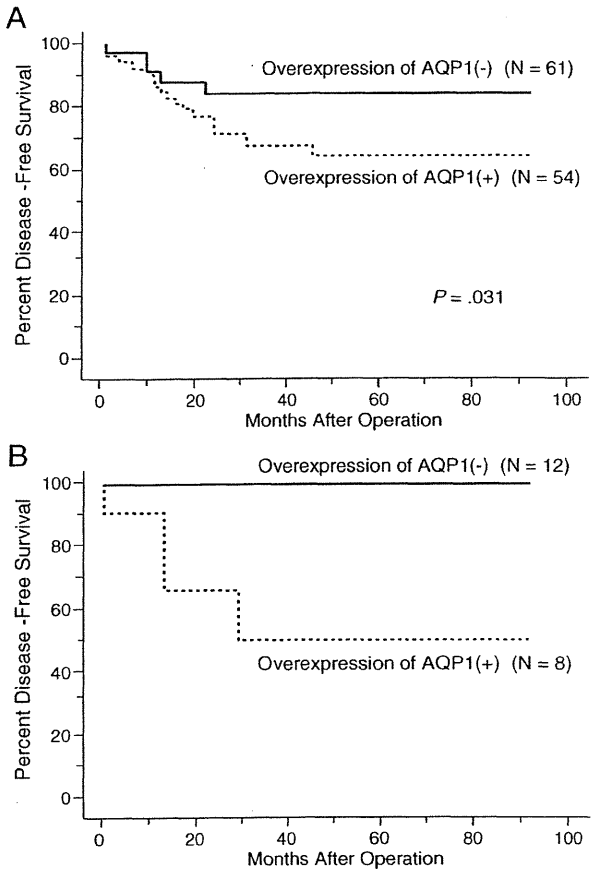

Fig. 6 A and B, Disease-free survival rates of lung cancer patients with or without AQP1 overexpression. A, Total lung cancer patients. B, Lung cancer patients with a micropapillary ADC component. A, Kaplan-Meier analysis reveals a significantly less favorable disease-free survival rate in patients with AQP1 overexpression compared with those without AQP1 overexpression (log-rank test, $P = .031$). The influence of AQP1 overexpression is particularly evident in patients with a micropapillary ADC component, although a log-rank score cannot be obtained because metastasis was not seen in any of the patients without AQP1 overexpression.

of AQP1 overexpression ($P = .055$; relative ratio, 3.049; 95% confident intervals, 0.975-9.523). AQP3 and 5 expression did not show any significant relation to postoperative metastasis ratios or prognosis.

No correlation was found between AQP1 and 5 overexpression and biological/prognostic markers including MIB-1 labeling index, p53 status, or CEA overexpression.

4. Discussion

The present study confirmed the hitherto reported findings concerning the expression of AQP1, 3, and 5 in human and animal lung tissue [7,9,20]. However, contrary to previous reports, we found that AQP1 was expressed in the apicolateral plasma membrane of type II pneumocytes, whereas both AQP1 and 5 were localized on the apical surface of BSE. The apicolateral AQP1 expression was particularly evident in reactive proliferating type II pneumocytes and AAH, which indicates that AQP1 expression may be up-regulated in type II pneumocytes in response to some stimulation. In lung cancer, nonmucinous BAC cells retained the apicolateral expression pattern of AQP1, as well as AQP3, as reported by Hoque et al [19] and Liu et al [20]. Localized AQP1 and 5 in the apical surface of BSE, as well as basolateral AQP3 expression [20], were maintained in mucinous BAC tumor cells except for goblet cell-type tumor cells. Thus, AQP expression and subcellular localization in lung cancer in essence seem to be determined by cellular differentiation of the tumor cells. Of note, the basolateral AQP5 expression in nonmucinous BAC cells and AAH is unique. In nonneoplastic lung tissues, neither type II pneumocytes nor Clara cells express AQP5, indicating that the acquisition of AQP5 expression might represent an early event in lung ADC development [21].

In the present study of AQP1 in nonneoplastic lung tissue, the protein expression was shown by Western blot, although the mRNA level was extremely low. This discrepancy is most likely caused by AQP1 expressed on cell membranes of red blood cells in the tissue, which scarcely have the message because of lack of nuclei.

We could discriminate 2 different AQP expression patterns: a subcellular polarized expression associated mainly with differentiation and an overexpression with loss of subcellular polarization and/or intracytoplasmic distribution. The intracytoplasmic distribution of AQPs seems to represent their enhanced localization in intracellular vesicles

Table 2 Univariate analysis of the adverse effect on disease-free survival rates of lung cancer patients (n = 115)

Parameter	RR	95% CI	*P* value
Age (>60 y)	1.006	0.963-1.051	.781
Sex (M)	1.425	0.605-3.460	.418
Smoking history	1.391	0.601-3.145	.441
Stage (I)	0.007	0.001-0.055	<.001 †
Tumor size (>2 cm)	1.413	0.518-3.823	.498
Histologic subtype (ADC)	0.797	0.244-2.716	.804
Histologic differentiation (G3,4) [a]	3.211	1.364-7.598	.041 *
CEA (>60%)	1.316	0.361-4.785	.677
p53 (>30%)	1.066	0.412-2.761	.895
MIB-1 labeling index (>10%)	2.911	1.061-7.983	.038 *
AQP1 overexpression	2.861	1.041-7.702	.041 *

Abbreviations: RR, relative ratio; CI, confident interval; M, male.
[a] Consisted of ADC (G3) and undifferentiated carcinoma (G4) because no case of SCC (G3) was included in the study.
* $P < .05$.
† $P < .01$.

[8]. These vesicles are reported to be trafficked to the plasma membrane following phosphorylation induced by intracellular signal transduction pathways activated in response to appropriate stimulation [17]. The overexpression patterns of AQP1 and 5 were found more frequently in invasive ADC than in BAC. AQP1 was demonstrated to be overexpressed quantitatively in invasive ADC by Western blotting. Analysis of ADC tumor tissues of mixed subtype by LCMD/real-time RT-PCR revealed that AQP1 gene expression was up-regulated in invading ADC cells compared with that in BAC cells, whereas AQP3 gene expression showed the opposite pattern. It is noteworthy that, in poorly differentiated ADC, invading tumor cells associated with fibroblastic reaction strongly expressed AQP1, in contrast to an almost total lack of AQP1 expression in expansively growing ones. These findings suggest that the overexpression of AQP1 and 5 in the tumor cells may play an important role in the aggressive growth of lung ADC, likely arising from derangements of gene regulation associated with the tumor progression. The lack of the correlation of AQP1 and 5 overexpression to proliferation, p53 status, or CEA production of lung cancer cells further supports the involvement in their invasive and metastatic potential.

The present study showed, for the first time, that AQP1 overexpression is related to high postoperative metastasis ratios and significantly shorter disease-free survival rates in lung cancer. The relation between AQP1 overexpression and metastatic potential was evident in ADCs. A significant correlation was also found in mucinous tumors and ADCs with a micropapillary component. ADC patients with a micropapillary ADC component overexpressing AQP1 showed remarkably poor disease-free survival rates, suggesting the involvement of AQP1 in the spread of the micropapillary component. Chae et al [21] reported that AQP5 expression is an independent prognostic factor in non–small cell lung cancer. In our study, however, neither total expression nor overexpression of AQP5 had any prognostic implications. Because the primary antibody applied and the immunostaining method used were the same for both studies, differences in either the number or composition of the subtypes of lung cancer investigated might have affected the results. These discrepancies should be examined in greater detail in future studies using larger number of cases with particular attention paid to AQP phosphorylation status because AQP5 phosphorylated at the cAMP-protein kinase consensus site located in a cytoplasmic loop plays a pivotal role in the up-regulation of cancer-associated pathways [29].

There are several lines of thinking regarding the molecular mechanisms of AQPs in cellular invasion. One is the water permeability hypothesis [3,6,7,15,30]. Experiments using mice lacking AQP1 and the forced expression of AQP1 in melanoma and breast cancer cell lines provided evidence that AQP1-dependent cell migration involves AQP1-facilitated water influx into dynamic cellular protrusions (lamellipodia) creating space for actin polymerization at the leading edge of migrating cells and contributing to invasiveness and extravasation of tumor cells as well as angiogenesis [6,15,30]. Another model implicates AQPs as a linker to adaptor molecules involved in activating signal transduction pathways that promote the epithelial mesenchymal transition [18,21,29]. Chae et al [21] showed that forced expression of AQP5, particularly in the phosphorylated form, increased the migration and invasion of human bronchial cells and that phosphorylated AQP5, through its SH3 binding consensus domain, interacted with the activated form of c-SRC, a nonreceptor cytoplasmic tyrosine kinase associated with an invasive and metastatic phenotype. AQP1 may be involved in actin cytoskeleton organization by interacting with Lin7/β-catenin to act as a scaffolding protein [18]. The demonstration of AQP1 in lamellipodia at the leading edge of invading ADC cells with fibroblastic reaction in the present study may support the water permeability role of AQP1, although the exact molecular mechanisms of AQPs in invading lung cancer cells need to be defined in vivo.

Our findings provide evidence that subcellular polarization of AQP1, 3, and 5 is closely associated with the cellular differentiation of lung cancer cells. The results also have provided insight into the involvement of AQP5 induction in carcinogenesis and of AQP1 overexpression in the invasive and metastatic growth of lung cancer, especially of ADC. In addition to in vitro approaches, future morphologic studies paying attention to subcellular polarization and expression levels should lead to a deeper understanding of the functional roles of AQP1 and 5 in the malignant progression of lung cancer.

References

[1] King LS, Agre P. Pathophysiology of the aquaporin water channels. Annu Rev Physiol 1996;58:619-48.
[2] Verkman AS, van Hoek AN, Ma T, et al. Water transport across mammalian cell membranes. Am J Physiol 1996;270:C12-30.
[3] Papadopoulos MC, Saadoun S, Verkman AS. Aquaporins and cell migration. Pflugers Arch-Eur J Physiol 2008;456:693-700.
[4] Mobasheri A, Marples D. Expression of the aquaporin 1 (AQP1) water channel in normal human tissues: a semi-quantitative study using tissue microarray technology. Am J Physiol Cell Physiol 2004;110: C529-37.
[5] Agre P, Kozono D. Aquaporin water channels: molecular mechanisms for human diseases. FEBS Lett 2003;555:72-8.
[6] Verkman AS. Knock-out models reveal new aquaporin functions. In: Beitz E, editor. Handbook of experimental pharmacology 190, aquaporins. Berlin, Germany: Springer-Verlag; 2009. p. 359-77.
[7] Verkman AS. Role of aquaporins in lung liquid physiology. Respir Physiol Neurobiol 2007;159:324-30.
[8] Liu H, Wintour EM. Aquaporins in development—a review. Reprod Biol Endocrinol 2005;3:18-28.
[9] Agre P. The aquaporin water channels. Proc Am Thorac Soc 2006;3: 5-13.
[10] Kageyama Y, Sasaki S, Yamamura Y, et al. Water channel protein subtype suggests the origin of renal cell carcinoma. J Urol 1996;156: 291-5.

[11] Saadoun S, Papadopoulos MC, Davies DC, et al. Increased aquaporin 1 water channel expression in human brain tumours. Br J Cancer 2002;87:621-3.
[12] Aishima S, Kuroda Y, Nishihara Y, et al. Down-regulation of aquaporin-1 in intrahepatic cholangiocarcinoma is related to tumor progression and mucin expression. Hum Pathol 2007;38:1819-25.
[13] Kang SK, Chae YK, Woo J, et al. Role of human aquaporin 5 in colorectal carcinogenesis. Am J Pathol 2008;173:518-25.
[14] Otterbach F, Callies R, Adamzik M, et al. Aquaporin 1 (AQP1) expression is a novel characteristic feature of a particularly aggressive subgroup of basal-like breast carcinomas. Breast Cancer Res Treat 2010;120:67-76.
[15] Verkman AS, Hara-Chikuma M, Papadopoulos MC. Aquaporins—new players in cancer biology. J Mol Med 2008;6:523-9.
[16] Saadoun S, Papadopoulos MC, Hara-Chikuma M, et al. Impairment of angiogenesis and cell migration by targeted aquaporin-1 gene disruption. Nature 2005;434:786-92.
[17] Woo J, Lee J, Chae YK, et al. Overexpression of AQP5, a putative oncogene, promotes cell growth and transformation. Cancer Lett 2008;264:54-62.
[18] Monzani E, Bazzotti R, Perego C, et al. AQP1 is not only a water channel: it contributes to cell migration through Lin7/beta-catenin. PLoS One 2009;e6167:8.
[19] Hoque MO, Soria JC, Woo J, et al. Aquaporin 1 is overexpressed in lung cancer and stimulates NIH-3T3 cell proliferation and anchorage-independent growth. Am J Pathol 2008;168:1345-53.
[20] Liu YL, Matsuzaki T, Nakazawa T, et al. Expression of aquaporin 3 (AQP3) in normal and neoplastic lung tissues. Hum Pathol 2007;38:171-8.
[21] Chae YK, Woo J, Kim MJ, et al. Expression of aquaporin 5 (AQP5) promotes tumor invasion in human non small cell lung cancer. PLoS One 2008;e2162:14.
[22] Travis WD, Garg K, Franklin WA, et al. Evolving concept in the pathology and computer tomography imaging of lung adenocarcinomas and bronchioloalveolar carcinoma. J Clin Oncol 2005;23:3279-87.
[23] Miyoshi T, Satoh Y, Okumura S, et al. Early-stage lung adenocarcinomas with a micropapillary pattern, a distinct pathologic marker for a significant poor prognosis. Am J Surg Pathol 2003;27:101-9.
[24] Colby TV, Noguchi M, Henschke C, et al. Adenocarcinoma. In: Travis WD, et al, editor. World Health Organization classification of tumours. Pathology & genetics of tumours of the lung, pleura, thymus and heart. Lyon, France: IARC Press; 2004. p. 35-44.
[25] Motoi N, Szoke J, Riely GJ, et al. Lung adenocarcinoma: modification of the 2004 WHO mixed type to include the major histologic subtype suggests correlations between papillary and micropapillary adenocarcinomas subtypes, EGFR mutations and gene analysis. Am J Surg Pathol 2008;32:810-27.
[26] Rami-Porta R, Crowley JJ, Goldstraw P. The revised TNM staging system for lung cancer. Ann Thorac Cardiovasc Surg 2009;15:4-9.
[27] Anami Y, Iijima T, Suzuki K, et al. Bronchioloalveolar carcinoma (lepidic growth) component is a more useful prognostic factor than lymph node metastasis. J Thorac Oncol 2009;4:951-8.
[28] Shima I, Katsuda S, Ueda Y, et al. Expression of matrix metalloproteinases in wound healing after glaucoma filtration surgery in rabbits. Ophthalmol Res 2007;39:315-24.
[29] Woo J, Lee J, Kim MS, et al. The effect of aquaporin 5 overexpression on the Ras signaling pathway. Biochem Biophys Res Commun 2008;367:291-8.
[30] Hu L, Verkmann AS. Increased migration and metastatic potential of tumor cells expressing aquaporin water channels. FASEB J 2006;20:1228-36.

（肺癌．2012;52:17-22）

ORIGINAL ARTICLE

肺腺癌の進展におけるアクアポリンの役割

町田雄一郎[1]・上田善道[2]・上野正克[1]・田中　良[1]・
相川広一[1]・薄田勝男[1]・佐川元保[1]・佐久間勉[1]

The Aquaporin Family: A Novel Player in the Progression of Adenocarcinoma of the Lung

Yuichiro Machida[1]; Yoshimichi Ueda[2]; Masakatsu Ueno[1]; Ryo Tanaka[1];
Kouichi Aikawa[1]; Katsuo Usuda[1]; Motoyasu Sagawa[1]; Tsutomu Sakuma[1]

[1]Department of Thoracic Surgery, [2]Department of Pathology, Kanazawa Medical University, Japan.

ABSTRACT —— ***Objective.*** Aquaporins (AQPs) are a family of small (-28 kDa/monomer) channel-forming membrane proteins that function as osmotically driven transepithelial and transcellular water transporters. To date, 13 homologous members have been identified in mammals. Recent studies using several varieties of aquaporin-gene knock-out mice have indicated previously unanticipated roles for AQPs, including cell cycle control and migration. In this review, we summarize the recent data on the involvement of AQPs in the progression of adenocarcinoma of the lung. ***Results.*** AQP1, 3, 4 and 5 were demonstrated in normal lung tissue with cell type-specific and polarized patterns. AQP1, 3 and 5 were frequently expressed in lung adenocarcinoma tissue subtypes. There were 3 recognized AQP-expression patterns: 1) a polarized expression of AQP1 and 3 in accordance with the differentiation of normal lung cells; 2) a polarized but aberrant expression of AQP5, and 3) the overexpression in the absence of any polarity of AQP1 and 5. Pattern 1) was seen predominantly in bronchioloalveolar carcinoma cells, of either non-mucinous or mucinous type, and decreased according to the progression of the disease. Pattern 2) was detected not only in bronchioloalveolar carcinoma cells, but also in atypical adenomatous hyperplasia cells, which suggested a relationship between AQP5 expression and the tumorigenesis of adenocarcinoma. Pattern 3) has been increasingly observed in the areas with micro-invasion, becoming prominent in the areas with widespread invasion, and correlated significantly with the decreased survival rates observed in adenocarcinoma patients. The oncogenic roles of each pattern were determined by *in vitro* studies using tumor cells with the AQP cells either knocked-in or knocked-out. Overexpressed AQP1 facilitated lamellipodia formation at the front line of the invasion, and AQP5 activated intracytoplasmic signal molecules, which play critical roles in cellular proliferation and epithelial mesenchymal transition (EMT). The involvement of AQP5 in the secretion of mucin in mucinous tumors and AQP1 in the aggressiveness of micropapillary components were also observed. The level of AQP4 expression was high in lung adenocarcinoma, and correlated significantly with a more favourable prognosis in adenocarcinoma patients. ***Conclusion.*** Several studies indicate that AQP1 and 5 are vital activators of the EMT of lung adenocarcinoma, suggesting that AQP can be a novel target molecule for counteracting the aggressiveness of lung adenocarcinoma.

(JJLC 2012;52:17-22)

KEY WORDS —— Lung adenocarcinoma, Aquaporin

Reprints: Yuichiro Machida, Department of Thoracic Surgery, Kanazawa Medical University, 1-1 Daigaku, Uchinada-machi, Kahoku-gun, Ishikawa 920-0293, Japan (e-mail: y-matti@kanazawa-med.ac.jp).

Received June 1, 2011; accepted January 13, 2012.

要旨 —— 目的． 細胞膜水輸送チャネルとして発見されたアクアポリン aquaporin（AQP）にがんの発生や進展に

金沢医科大学 [1]呼吸器外科学，[2]病理学 II.
別刷請求先：町田雄一郎，金沢医科大学呼吸器外科学，〒920-0293 石川県河北郡内灘町大学 1-1（e-mail: y-matti@kanazawa-med.ac.jp）.

受付日：2011 年 6 月 1 日，採択日：2012 年 1 月 13 日.

関わる新規機能の存在が近年提唱された．本稿では多様な肺腺癌亜型におけるAQPの発現と進展への関与に関する知見を紹介する．**結果．**肺癌ではAQP1，3，4，5が腺癌細胞に発現する．その発現は，1)細胞分化に相当する極性を有するAQP1，3の発現，2)極性は保たれるが正常肺では認められないAQP5の異所性発現，3)極性を喪失したAQP1，5の過剰発現に区分される．1)は細気管支肺胞上皮癌に高頻度で，進展に伴い減少する．2)は肺胞上皮癌のみならず異型腺腫様過形成でも見られ，腫瘍発生に関係していると考えられる．3)は微小浸潤部から観察され始め，進展とともに頻度を増し，生命予後と有意な関連を示す．AQP1は浸潤先進部での発現亢進と浸潤部lamellipodia細胞膜での発現を介した，AQP5は細胞増殖や上皮間質移行関連分子の活性化を介した肺腺癌の浸潤・転移能亢進への関与が示唆されている．AQP5の発現と粘液産生性肺癌の進展，AQP1の過剰発現と微小乳頭状成分の侵襲性との関連性も認められる．また，AQP4は肺腺癌で発現レベルが高く，生命予後良好因子となる．**結論．**AQP1，5は肺腺癌の進展に関わる重要分子の一つと考えられ，新たな進展阻止法の確立のための標的分子となる可能性が示唆される．

索引用語——肺腺癌，アクアポリン

はじめに

アクアポリンaquaporin(AQP)は細胞膜を介した水輸送を担うチャンネル分子として1992年にPrestonらにより発見された.[1] 哺乳類では現在まで13種類がクローニングされ，その局在，生理的機能や疾患との関連が明らかにされてきた.[2] 近年，ノックアウトマウスを用いた研究から，AQPは水輸送以外に予想外の新たな機能を有することが明らかになり，特に，増殖や細胞移動・浸潤能などがんの発生や進展に関わる機能が注目され，現在，精力的に研究が展開されている.[3]

肺癌はがん死亡の首座を占め，その発生や進展に関わる分子機構の解明は最優先の研究課題の一つである．特に，最近，腺癌の増加が男女ともに著しい．肺腺癌には，肺胞上皮置換性増殖lepidic growthを示す異型腺腫様過形成と細気管支肺胞上皮癌，その一部に小さな浸潤病巣を伴ういわゆる微小浸潤癌，そして広範浸潤性高分化腺癌，低分化腺癌へと連なるスペクトラムの存在に加え，経気道転移を特徴とする粘液産生性癌や高侵襲性を呈する微小乳頭状腺癌など多彩な組織亜型が存在する.[4] これらの腺癌亜型の侵襲性と進展に関わる分子機構についての詳細な情報は未だ乏しい．

今回，腫瘍発生・進展との関連が注目されているAQPに関して，その肺腺癌亜型での発現と侵襲性や進展への関与に関する最新の情報を自験データも交え解説するとともに，今後の様々ながんの制御に向けた研究のための新たな視点を提供したい．

細胞膜水輸送チャンネル分子AQP

水は物質の輸送や生化学的反応の媒体となる生体における重要分子であり，細胞膜を介した迅速な輸送が求められる．リン脂質二重層からなる生体膜は単純な拡散では説明できない水分子輸送能を有するため，水分子特異的なチャンネルの存在が100年以上前から想定されていた.[1] 1992年，Agreらのグループは，赤血球細胞膜に分子量28 kDaの小型蛋白（CHIP28）が多く存在することを発見した.[1] この分子は浸透圧勾配に従って水分子を選択的に通すチャンネルとしての機能を有することが明らかとなり「アクアポリン(aquaporin)」と名づけられた．

AQPは小穴を中心に螺旋状ドメイン6個が輪状に配列する構造をとり，細胞膜では通常4分子が集合体を形成している．水分子がかろうじて通過できる直径3Åの中心小穴による通過分子サイズの制限のほか，静電性反発や双極子結合を介した水分子の通過促進など浸透圧を介した選択性の高い，かつ迅速な水輸送を可能にする機構が原子レベルで解明されている.[5] 哺乳類においては現在まで13種類の異なる分子種がクローニングされ，その組織分布・局在，生理学的機能や疾患との関係に関する情報が集積されている（Table 1）．呼吸器系ではAQP1，3，4，5の4種類の発現がこれまで報告されている.[2] 肺胞では，AQP1は毛細血管に発現し細胞を介した水輸送に関わる．AQP3はII型肺胞上皮の，AQP5はI型肺胞上皮の先端部細胞膜に発現し，特にAQP5は肺胞内水分移動に関係すると考えられている.[6] 気道系では，気管支線毛上皮の外側側底部細胞膜にAQP4が，基底細胞にAQP3が発現している．AQP5は気管支線毛上皮と粘膜下腺細胞の先端部細胞膜に発現する．さらに我々は，活動性II型肺胞上皮と気管支線毛上皮の頭頂部におけるAQP1の発現を明らかにした.[7] 気管支粘膜の杯細胞にはAQPの発現はこれまで認められていない．

肺腺癌におけるAQPの発現

肺癌組織におけるAQPの発現に関して，Hoqueら[8]によるAQP1の，Liuら[9]によるAQP3の，Warthら[10]によるAQP4の，Chaeら[11]によるAQP5の発現解析結果が報告されている．我々は128例の腺癌を含む肺癌

Table 1. Type, Location, and Function of Aquaporins (AQPs)

Molecular type	Tissue location	Function
AQP0	Lens	Lens osmoregulation (water transport, an adhesion factor)
AQP1	Red blood cells, Capillary endothelium, Kidney proximal tubules	Transcell membrane moisture transportation, Urine concentration
	Intrahepatic bile duct, Gallbladder, Ciliary body, Choroid plexus	Biligenesis, Cerebrospinal fluid production, Aqueous humor production
AQP2	Kidney collecting tubules	Vasopressin-dependent urine concentration
AQP3*	Red blood cells, Colon, Kidney, Lung, Liver, Pancreas, Skin	Urine concentration, Glandular secretion, Intracellular glycerol intake
AQP4	Neuroglia, Bronchial epithelium	Blood vessel/brain barrier functional regulation
AQP5	Salivary gland, Lacrimal gland, Bronchial gland, Alveolar epithelium	Glandular secretion, Intra-alveolar water absorption
AQP6	Glomerulus epithelial cells, Proximal tubules, Collecting tubules	Urine concentration
AQP7*	Sperm, Fat cells, Kidney	Glycerol intake of fat cells
AQP8	Pancreas, Colon, Liver, Kidney, Testis	Produce sperm, Colic water absorption, Bile levels adjustment
AQP9*	Neuroglia, Fat cells, White blood corpuscles	Glycerol intake in cells
AQP10*	Duodenum, Jejunum	Small intestinal hydration/small molecule absorption
AQP11	Kidney proximal tubules	Vesiculous form of cell maintenance
AQP12*	Pancreatic acinus cells	Digestive enzyme secretion

* aquaglyceroporin.

160症例でのAQP1, 3, 5の発現解析を行った.[7] 扁平上皮癌では約30%の症例で基底細胞の側底部にAQP3の発現が観察されるが, AQP1, 5の発現はほとんど認めない. AQP1, 3, 5とも腺癌細胞において発現頻度が高く, 特にbronchioloalveolar carcinoma (BAC) で高い発現頻度を示す (AQP1 96%, AQP3 100%, AQP5 76%).[7-9,11] 我々はこれまでの報告と自験データを総合し, 肺腺癌におけるAQP1, 3, 5の発現は3つのパターンに分類されることを見いだした. 1)腫瘍細胞の分化と関連する極性が保たれた発現, 2)極性は保たれているが腫瘍細胞の分化では説明できない異所性発現, 3)極性の喪失を伴う過剰発現の3種で, 3)ではしばしば細胞内陽性発現も伴う. 通常のBAC-微小浸潤癌-広範浸潤性高分化腺癌-低分化腺癌スペクトラムでは, BACで活動性II型肺胞上皮への分化に相当するAQP1の先端部細胞膜のパターンの発現を, II型肺胞上皮あるいはClara細胞への分化に相当するAQP3の先端部細胞膜あるいは外側側底部細胞膜のパターンの発現を認める. AQP5は外側側底部細胞膜への局在性発現を呈する. 正常末梢肺では, AQP5はI型肺胞細胞の先端部細胞膜に発現するがII型肺胞上皮やClara細胞には発現しない. BACにおけるAQP5の発現は2)の腫瘍化に伴う異所性発現と考えられる. AQP5の異所性発現はAAHでも観察される. 腺癌微小浸潤部ではAQP3の発現は低下するのに対して, AQP1, 5では極性を喪失し細胞全周性細胞膜における発現亢進を認めるようになる. 広範浸潤性高分化腺癌や低分化腺癌ではAQP3の発現はさらに低下する一方, AQP1, 5は細胞質内発現も伴う極性を喪失した過剰発現を示す (Figure 1). 特に, AQP1は腫瘍浸潤先端部での発現亢進が顕著で, さらに, 先進部のlamellipodiaに一致する細胞突起の細胞膜にも発現が認められる. 興味深いことに, 低分化腺癌においては, 間質の反応性増生を伴う浸潤性発育を呈する浸潤型は浸潤先進部に強いAQP1の過剰発現を認めるのに対して, 肺胞腔内を充満性に発育し間質増生を伴わない膨張型では腫瘍細胞におけるAQP1発現は見られない. この浸潤部腺癌細胞におけるAQP1の発現亢進とAQP3の発現低下は腫瘍組織を用いたwestern blotとlaser captured-microdissection/real time RT-PCRによる解析で蛋白ならびにmRNAでも確認されている.[7]

この3種類のAQPの発現パターンのうち, AQP1の極性の喪失を伴う過剰発現が腺癌の術後転移発生や生存率と有意な関連性を示す.[7] Warthらは AQP4発現陽性の肺腺癌患者が予後良好であり, 重要な予後因子であることを報告している.[10] Chaeらは3種の発現パターンには区分していないがAQP5の発現亢進と生命予後との有意な関連を報告している.[11]

AQP1とlamellipodia形成促進を介した運動能との関係

がん細胞の運動はアメーバー様突起形成を特徴とするelongated cell motilityと突起形成を認めないrounded

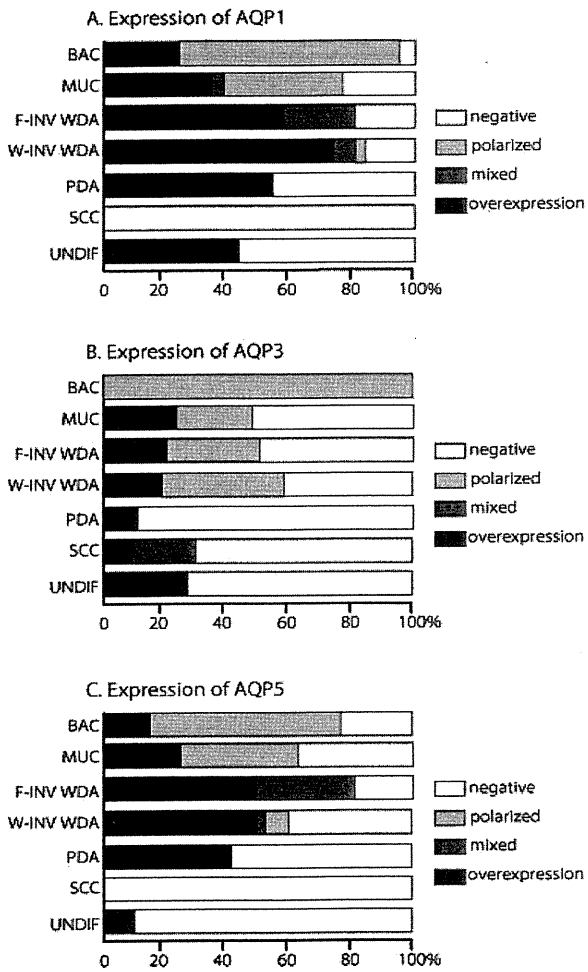

Figure 1. Expression patterns of AQP1, 3 and 5 in lung cancer. Gray shows the polarized cell membrane expression similar to normal cells in AQP1, 3, and the polarized but aberrant expression of apicolateral or basolateral in AQP5. Black shows cell membrane overexpression in the absence of a polarity, with the intracytoplasmic expression. BAC; bronchioloalveolar carcinoma of non-mucinous type, MUC; mucinous tumor, either BAC or mixed subtype, F-INV WDA; focally invasive adenocarcinoma of mixed subtype with a predominant BAC component, W-INV WDA; adenocarcinoma of mixed subtype comprising widespread invasive well- to moderately differentiated adenocarcinoma components, PDA; poorly differentiated adenocarcinoma, SCC; squamous cell carcinoma, UNDIF; small and large cell carcinoma.

bleb-associated motility の2種類に大きく分けられる．後者がRho依存性なのに対して前者はRac依存性，後者はプロテアーゼの活性化は伴わないのに対して前者は先進部でのプロテアーゼの活性化とF-actin重合を伴う．[12] Elongated cell motilityでは，先ず運動方向へのlamellipodiaと呼ばれる厚さ約300 nmの平坦な，細胞小器官を含まない細胞膜の突出が形成される．このlamellipodia形成時には局所的な細胞体積の増加が必須であり，そこでは従来Na/Kイオン交換運動による水移動が想定されていたが，それだけでは迅速な体積の変化は完全には説明できなかった．[13] Saadounらは AQP1遺伝子ノックアウトマウス由来の血管内皮細胞を用いた検討からAQP1は血管内皮細胞の運動性に関係し，運動方向の細胞先進部でのruffle形成を亢進させることを報告した．[14] ネズミの悪性黒色腫細胞と乳癌細胞への遺伝子導入によるAQP1の過剰発現により，*in vitro*での浸潤能亢進に加え，ヌードマウスの尾静脈注入による肺転移形成も亢進する．[15] さらに，Huら[15]やPapadopoulousら[16]はこの腫瘍細胞の移動・浸潤過程におけるlamellipodiaの細胞突起先端部細胞膜におけるAQP1を介した急速な水の流入を細胞生理学的に明らかにした．細胞移動先進部の細胞突起部ではアクチンの脱重合が生じ，このアクチン分子による浸透圧増加が細胞膜を介した急速な水分子の流入の駆動力となると推測されている．[16]

一方，単一細胞の移動と関係するもう一つの細胞膜突起構造であるfilopodia形成にはAQP9が関係している．AQP9により水の流入が起こり，アクチンフィラメントは伸長し，PKC結合によりPar3・Par6・Cdc42が三量体を形成する．この三量体がWASP抑制を解きアクチンポリメリゼーションを起こす．また，この三量体はIRSp53/Menaを活性化させ，活性化されたWASPとIRSp53/Menaは，filopodiaを形成させることが明らかになった．[17]

CraneらはAQP1の過剰発現によるAQP1の細胞形状変化部，特に浸潤先端部lamellipodiaへの迅速な供給を示した．[18] 移動細胞先端部，すなわちlamellipodia部ではphosphatidylinositol-3 kinase（PI3K）をはじめとする複数の細胞内シグナル伝達分子が活性化されていることも観察されている．[19] 骨髄由来間葉系幹細胞，マクロファージをはじめとしてがん細胞の微小環境から分泌されるケモカインや増殖因子，matrix metalloproteinaseをはじめとするタンパク分解活性により細胞外基質から遊離される増殖因子など複数の細胞外シグナルが移動細胞先端部において細胞内シグナルとして増幅され，その一つの効果としてAQP発現亢進を介したlamellipodia形成，移動・浸潤能の亢進が生じるものと考えられる．[20] AQP1発現亢進によるlamellipodiaの形成促進はがん細胞の迅速な周囲組織への浸潤性増殖だけでなく，腫瘍血管新生の亢進にも関係し，がんの転移形成に重要な働きをする．[3] この他，AQP1に関しては，足場蛋白（scaffolding protein）として機能するLin7/β-catenin複合体と関係しアクチン系細胞骨格形成に関与するという報告もあ